ELSEVIER

Atmospheric Research 59–60 (2001) 373–392

ATMOSPHERIC RESEARCH

www.elsevier.com/locate/atmos

A large-eddy simulation study of cumulus clouds over land and sensitivity to soil moisture

Jean-Christophe Golaz *, Hongli Jiang, William R. Cotton

Department of the Atmospheric Science, Colorado State University, Fort Collins, CO 80523-1371, USA

Received 10 January 2001; received in revised form 19 June 2001; accepted 12 July 2001

Abstract

A series of large-eddy simulations (LES) of non-precipitating cumulus clouds over land was performed. These simulations were idealized from observed conditions at the Southern Great Plains ARM site on 21 June 1997 and were intended to investigate the effect of initial soil moisture on the structure of the cloudy boundary layer. The surface fluxes were either dominated by latent heat or sensible heat flux, with the transition between one regime and the other occurring over a very narrow soil moisture range. The effect on clouds was mixed. Cloud fraction was nearly identical throughout all experiments. Simulations with dominant sensible heat fluxes led to more turbulent boundary layers and higher cloud bases. Simulations dominated by latent heat flux tended to have fewer but stronger updrafts in the cloud layer.

Keywords: Boundary layer clouds; Cumulus; Surface–atmosphere interaction; Soil moisture

1. Introduction

Large-eddy simulation (LES) models have been widely used as numerical tools to study the evolution of the atmospheric planetary boundary layer (e.g. Deardorff, 1972; Moeng, 1984). These models have the capability to explicitly resolve the large-scale turbulent eddies in the boundary layer while parameterizing the effect of the smaller, unresolved and less energetic eddies. To resolve the large-scale eddies, typical grid spacings used in LES are of the order of 100 m or less. A critical review of this modeling approach can be found in Mason (1994).

* Corresponding author.
E-mail address: golaz@atmos.colostate.edu (J.-C. Golaz).

0169-8095/01/$ - see front matter
PII: S0169-8095(01)00113-2

Many LES studies have focused on the structure of turbulence and statistical properties of clear convective boundary layers (e.g. Deardorff, 1974; Moeng and Wyngaard, 1984, 1988; Schmidt and Schumann, 1989). Others have focused on marine stratocumulus-topped boundary layers (e.g. Moeng et al., 1996 and references therein) and cumulus boundary layers (e.g. Cuijpers and Duynkerke, 1993; Cuijpers et al., 1996; Brown, 1999; among others).

LES models have also been used to investigate the interaction between the land surface and the structure of the turbulence in the boundary layer. Avissar et al. (1998) evaluated the LES option of the Regional Atmospheric Modeling System (RAMS). Using data from the First International Satellite Land Surface Climatology Project Field Experiment (FIFE), they found that the model performed well and was capable of reproducing observed atmospheric profiles. They also concluded that small-scale landscape heterogeneity and topography had only a small to moderate impact on the structure of the boundary layer. In another study, Avissar and Schmidt (1998) showed that for surface patchiness with a length scale of the order of 10 km or less, the heterogeneities in the land surface had only a moderate impact on the structure of the boundary layer. At larger scales, however, landscape heterogeneities were found to have a significant impact by generating mesoscale circulations. Many other studies have studied the impact that spatial distribution of vegetation and soil moisture can have on cumulus convection and rainfall. A review of those studies can be found in Pielke (2001).

Lewellen et al. (1996, hereafter LLY1996) conducted a series of LES to investigate the sensitivity of stratocumulus boundary layer clouds to the surface Bowen ratio, the role of cloud top radiative cooling, strength of cloud top inversion, wind shear, and relative boundary layer thickness. They found that for a given surface heating, sensible heat dominated surface fluxes were much more efficient at generating buoyancy-driven turbulence. As surface latent heat flux increased, cloud base tended to be lower and updrafts to be fewer and stronger. Large variations in maximum cloud fraction were observed between their various simulations, and a good correlation between maximum cloud fraction and relative humidity was found.

The research described in this paper focuses on non-precipitating cumulus clouds forming on top of a convective boundary layer. The objective is to investigate the sensitivity of a cumulus-capped boundary layer to initial soil moisture content through an idealized case study. Two questions are of particular interest: (i) How does the initial soil moisture content affect the partitioning of available energy into surface sensible and latent heat fluxes? (ii) How does this partitioning affect the overall dynamics of the cloudy boundary layer? This includes the influence of surface fluxes on the structure of the cumulus clouds, such as cloud base and depth, cloud fraction and liquid water content, and in-cloud turbulence. Numerical simulations based on observations at the Southern Great Plain (SGP) ARM site on 21 June 1997 are used to address these questions. Where possible, comparisons between the simulations are made with observational data; however, this work should not be regarded as a rigorous case study, but rather as a series of idealized sensitivity experiments.

This paper is organized as follows: Section 2 gives a description of the case used in this study and the sensitivity experiments conducted. Details of the numerical model are also outlined. Section 3 presents results from the surface fluxes and their sensitivity to the initial soil moisture. In Section 4, a description of the dynamics of the cloudy boundary layer is

presented and differences among the various sensitivity runs are presented. Similarities and differences between this work and previously published results are discussed. Finally, Section 5 summarizes the major findings of this research.

2. Case description

The 6th GEWEX Cloud System Study (GCSS) boundary layer clouds working group intercomparison workshop focused on a case of daytime, non-precipitating cumulus clouds over land developing on top of an initially clear convective boundary layer. This case was based on observations taken from the SGP ARM site on 21 June 1997. A complete description of the intercomparison case set-up can be found at ftp://email.meto.gov.uk/pub/apr/arm/. We will only briefly outline some of the features of this case. The models were initialized at 1130 UTC (530 LST) with profiles of potential temperature, total water mixing ratio, and horizontal winds that were idealized from observed soundings at the ARM site. The initial profiles of potential temperature and total water mixing ratio are shown in Fig. 1 along with the observed soundings from the ARM site. This comparison shows that the initial profiles do not closely match the observations for the same time period. They were idealized by the organizers of the intercomparison workshop to account for a significant cooling from 500 to 2000 m, between 1130 and 1430 UTC not provided by in the diagnosed large-scale forcings. As a result, the idealized profiles are a compromise between the observations from 1127 and 1428 UTC. The potential temperature profile was also modified to increase the stability above 2500 m in order to prevent any clouds from reaching the imposed damping layer located below the model tops. Initial constant with height wind profiles of $u = 10$ m/s and $v = 0$ m/s were used. Modelers were required to impose time-varying surface latent and sensible heat fluxes based on observations. Large-scale heat and moisture forcings intended to mimic advective and radiative forcings were also imposed. No interactive radiation transfer calculation was required for the intercomparison.

As participants in the intercomparison, we performed two simulations using the LES version of the Regional Atmospheric Modeling System (RAMS) (Pielke et al., 1992; Cotton et al., submitted for publication). The domain size was 6700 m in the two horizontal directions and 4400 m in the vertical. As it is customary for LES models, periodic boundary conditions were used in the horizontal directions. The subgrid-scale fluxes were computed following Deardorff (1980) using a prognostic equation for the subgrid-scale turbulence kinetic energy (TKE). Condensation was accounted for by a simple non-precipitating saturation adjustment scheme in which cloud water is diagnosed as the difference between total water mixing ratio and saturation mixing ratio. The first simulation was carried out with a grid spacing of 100 m in the horizontal directions and 40 m in the vertical. A second, higher resolution simulation was performed with a horizontal grid increment of 67 m. Results from those two experiments agreed well with each other and we therefore retained a lower resolution for additional experiments. Validity of the simple saturation adjustment condensation scheme was tested by performing one simulation with a bulk microphysics scheme (Walko et al., 1995). Results were not found to be significantly different for this particular case. Comparisons of the results from various

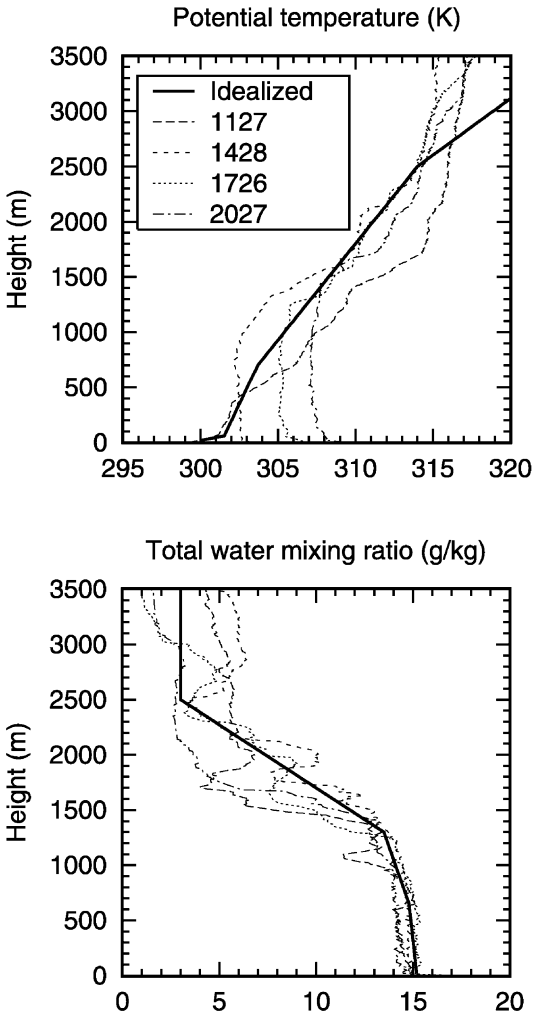

Fig. 1. Initial profiles of dry potential temperature, total water mixing ratio for the idealized intercomparison case starting at 1130 UTC and observed profiles at 1127, 1428, 1726, and 2027 UTC.

models presented at the intercomparison workshop will be the subject of an upcoming publication.[1] It should be noted that the results obtained with RAMS compared favorably with other LES models.

After validating the model results for this idealized case against other numerical models, we conducted a series of sensitivity experiments in which the imposed surface fluxes and radiative tendencies were replaced with an interactive land–surface model,

[1] A.R. Brown, personal communication.

Table 1
Description of the sensitivity experiments

Experiment	Initial soil moisture (kg_{water}/kg_{soil})	Soil relative wetness (%)
Exp 12.5	0.125	42.0
Exp 13.3	0.133	44.5
Exp 14.0	0.140	47.0
Exp 14.8	0.148	49.5
Exp 15.5	0.155	52.0
Exp 18.5	0.185	62.0

LEAF-2 (Walko et al., 2000), and a two-stream radiative transfer code (Harrington, 1997), respectively. The goal of those additional experiments was to investigate the sensitivity of the surface fluxes and resulting cloud field to the initial soil moisture content. Topsoil moisture is measured at five different locations around the SGP ARM site. Values measured at 1130 UTC on 21 June 1997 ranged from approximately 0.12–0.22 kg_{water}/kg_{soil}. Silty clay loam soil type was chosen to be representative of the area. It has a soil moisture saturation content around 0.3 kg_{water}/kg_{soil}, corresponding to soil relative wetness values in the range from 40% to 73%. We used this observed range as a guideline for designing our sensitivity experiments. Table 1 summarizes the simulations that were conducted. The mixed-farming vegetation category was used in LEAF-2. All simulations were initialized with uniform soil moisture, both in the horizontal and vertical dimensions. Because of the small domain size and strong horizontal winds, horizontal surface heterogeneities would not be expected to play a significant role in this case according the findings of Chen and Avissar (1994) and Avissar and Schmidt (1998). Since only surface values of soil moisture were available, we made the simplifying assumption that the soil moisture was uniform with depth. This assumption might not be realistic, depending on the meteorological conditions prevailing during the preceding days. However, the goal of this study was not to exactly reproduce measured surface fluxes, but rather to conduct a sensitivity analysis on the influence of soil moisture on the surface fluxes and the development of the cloudy boundary layer.

3. Results: surface fluxes

The land–surface model interacts with the atmosphere mostly through the surface energy fluxes and the partitioning of the available energy between latent and sensible heat fluxes. Time evolution of domain-averaged fluxes are shown in Fig. 2. The two experiments with the highest soil moisture (Exp 18.5 and 15.5) produce nearly identical surface fluxes with the latent heat flux reaching a maximum of 550 W/m^2 and a sensible heat flux of 80 W/m^2. On the other side of the soil moisture spectrum, the two driest experiments (Exp 12.5 and 13.3) also produce nearly identical fluxes but with a very different partitioning. The maximum latent heat flux is now of the order of 180 W/m^2, with most of the available energy being shifted to sensible heat, which reaches a maximum value around 370 W/m^2. The transition between those two regimes, one latent heat dominated

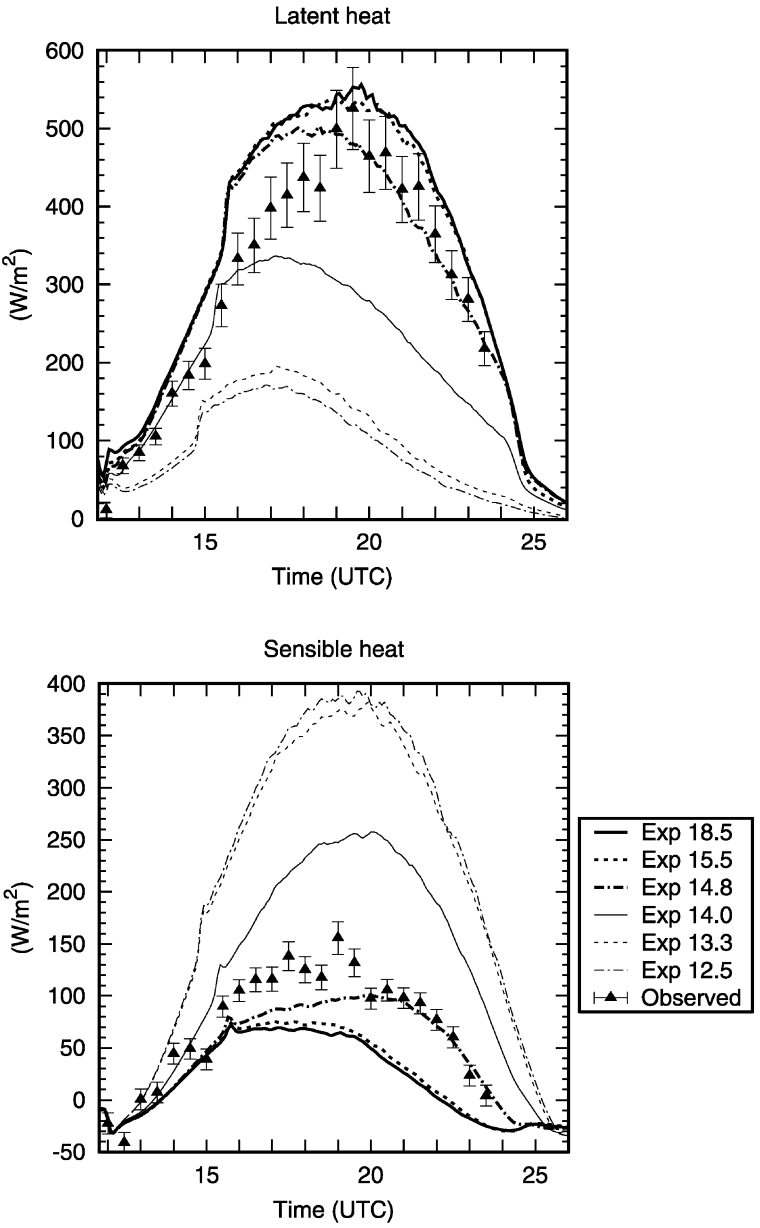

Fig. 2. Time evolution of domain-averaged surface latent and sensible heat fluxes. Observations are shown with triangles.

and one sensible heat dominated occurs in a very narrow soil moisture range between Exp 13.3 and 15.5. Two simulations fall into this category, Exp 14.8 and 14.0. Exp 14.8 is the one which most closely produces fluxes resembling observations with maximum latent

heat flux around 500 W/m^2 and sensible heat flux around 100 W/m^2. The agreement with measured fluxes is good during the second half of the day, but not as good during the first half of the day when Exp 14.8 overestimates latent heat flux and underestimates sensible heat flux. This difference is likely due to the simplifying assumption of uniform soil moisture with depth, which might have led to an overestimation of deep soil moisture within the vegetation root zone.

To better understand the sharp transition that occurs in surface heat fluxes as soil moisture varies, it is of interest to look at the various contributions to the total latent heat flux. In LEAF-2, four different processes contribute: the transpiration through the plant's stomata, the evaporation from the ground, and the evaporation and condensation of moisture on the vegetation. The latter two processes are negligible in our simulations due to the absence of precipitation. For the relatively moist experiments (18.5 and 15.5), vegetation transpiration is the dominant contribution to the total latent heat flux with approximately 80% of the total. For the dry simulations (12.5 and 13.3) transpiration does not contribute significantly and virtually all the latent heat comes from direct evaporation from the ground. To synthesize the influences of the initial soil moisture on the partitioning of available energy, the average evaporative fraction was computed for all simulations between 1800 and 2100 UTC. The evaporative fraction, EF, is defined as:

$$\mathrm{EF} = \frac{\lambda E}{H + \lambda E} = \frac{1}{1 + \beta} \tag{1}$$

where λE is the latent heat flux, H the sensible heat, and β the Bowen ratio. The relation between EF and initial soil moisture is shown in Fig. 3. The driest simulations, Exp 12.5

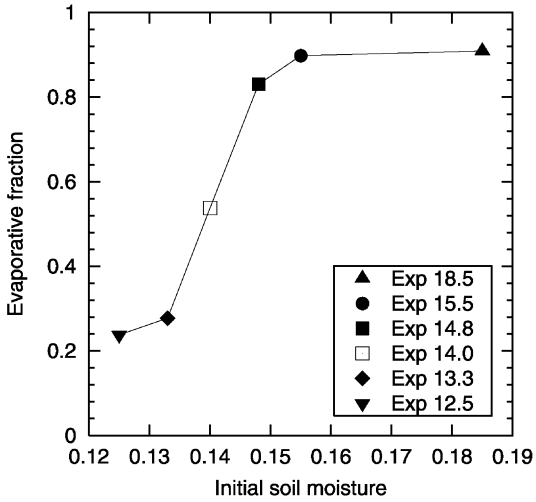

Fig. 3. Domain-averaged evaporative fraction for all experiments averaged between 1800 and 2100 UTC.

and 13.3, have low evaporative fractions in the range 0.2–0.3, whereas the moister simulations, Exp 14.8, 15.5, 18.5, have fractions upwards of 0.8. Exp 14.0 is a transition point between low and high EF values with a value of 0.54, reflecting a near equal partitioning of the available energy between sensible and latent heat fluxes. As can be seen from Fig. 3, the transition between low and high values of EF is sharp and occurs over a narrow range of soil moisture around 0.14.

This change in EF is caused by the sharp reduction of the vegetation contribution to the latent heat flux in the driest experiments, and a resulting redistribution of the available energy into sensible heat flux. In LEAF-2, the vegetation transpiration is controlled by the stomatal conductance, g_{sr}, which is modeled after Avissar and Pielke (1991):

$$g_{sr} = \Omega[\, g_{sm} + (g_{sM} - g_{sm}) f_R f_T f_V f_\psi] g_{sM} \tag{2}$$

where Ω is the leaf age function, g_{sm} and g_{sM} the minimum and maximum stomatal conductances which, respectively occur when the stomata are closed or completely open. Each of the f_i functions quantifies the influence of an environmental factor on the conductance, with f_R the solar radiation, f_T the leaf temperature, f_V the vapor pressure difference between leaf and canopy air, and f_ψ the soil water potential (SWP) in the root zone. Each function f_i is expressed in the form:

$$f_i(\chi_i) = \frac{1}{1 + \exp(-S_i(\chi_i - \chi_{bi}))} \tag{3}$$

with the constants S_i and χ_{bi} shown in Table 2 as in Lee (1992).

An analysis of the values of those functions in the land–surface model for all simulations revealed that the soil moisture was the environmental factor responsible for the limitation of the vegetation contribution to the latent heat flux in the driest experiments. The SWP response function f_ψ is shown in Fig. 4, along with markers indicating the initial SWP for all simulations. As can be seen from this figure, the response function has a vary sharp drop-off around a SWP value of -10^6 Pa. Simulations with highest soil moisture (Exp 18.5, 15.5) have SWPs that lie to the left of the drop-off of the response function. The driest experiments (Exp 12.5 and 13.3) on the other hand, lie to the right of the transition, implying that stomata conductance is limited by the lack of soil moisture. For this series of sensitivity experiments, the sharp

Table 2
Constants quantifying the environmental response functions (Eq. (3))
From Lee (1992).

Environmental factor	Units	χ_{bi}	S_i
Radiation	W/m^2	196	0.047
Temperature (cold range)	°C	8.33	0.258
Temperature (hot range)	°C	36.97	-0.124
Vapor pressure difference	Pa	4850	-0.0051
Soil water potential	Pa	-1.07×10^6	7.42×10^6

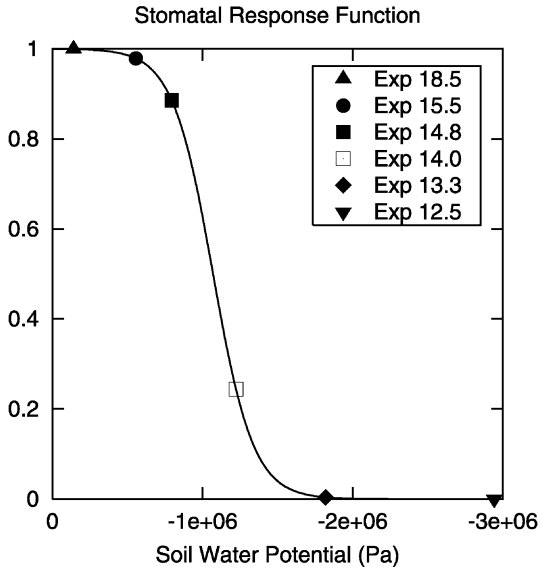

Fig. 4. Stomatal response function to soil water potential (solid line). Markers indicate initial SWP values for the sensitivity experiments.

transition between low and high values of EF as a function of initial soil moisture (Fig. 3) is a direct result of the specific choice of the stomatal response function to SWP (Fig. 4).

4. Results: effects on clouds

We now turn our attention to the effect of the various soil moisture contents on the cloudy boundary layer. Fig. 5 shows the time evolution of cloud base and cloud top, which are defined as the lowest, and respectively highest, model levels where a non-zero cloud water amount exists. Measured cloud base at the ARM site using a Belfort ceilometer and a micro-pulse lidar are shown in Fig. 6. According to cloud base observations, the first clouds appear around 1430 UTC and the last ones dissipate around 2330 UTC. This is similar for the simulations where clouds form approximately 3 h after the beginning of the simulations, between 1500 and 1600 UTC and dissipate around 2400 UTC. The moist simulations (Exp 18.5 and 15.5) have an initial cloud base located around 600 m, whereas the driest experiments (Exp 13.3 and 12.5) have an initial cloud base approximately 300 m higher. These differences become much larger during the course of the day. Changes in cloud top height are not as pronounced; the driest simulations tend to produce cloud tops approximately 500 m higher than the moister experiments. Change in cloud base height between the end and the beginning of the convection is shown in Table 3 for the simulations and the measured values. The driest experiments have very large increases in cloud base height, with more than 1000

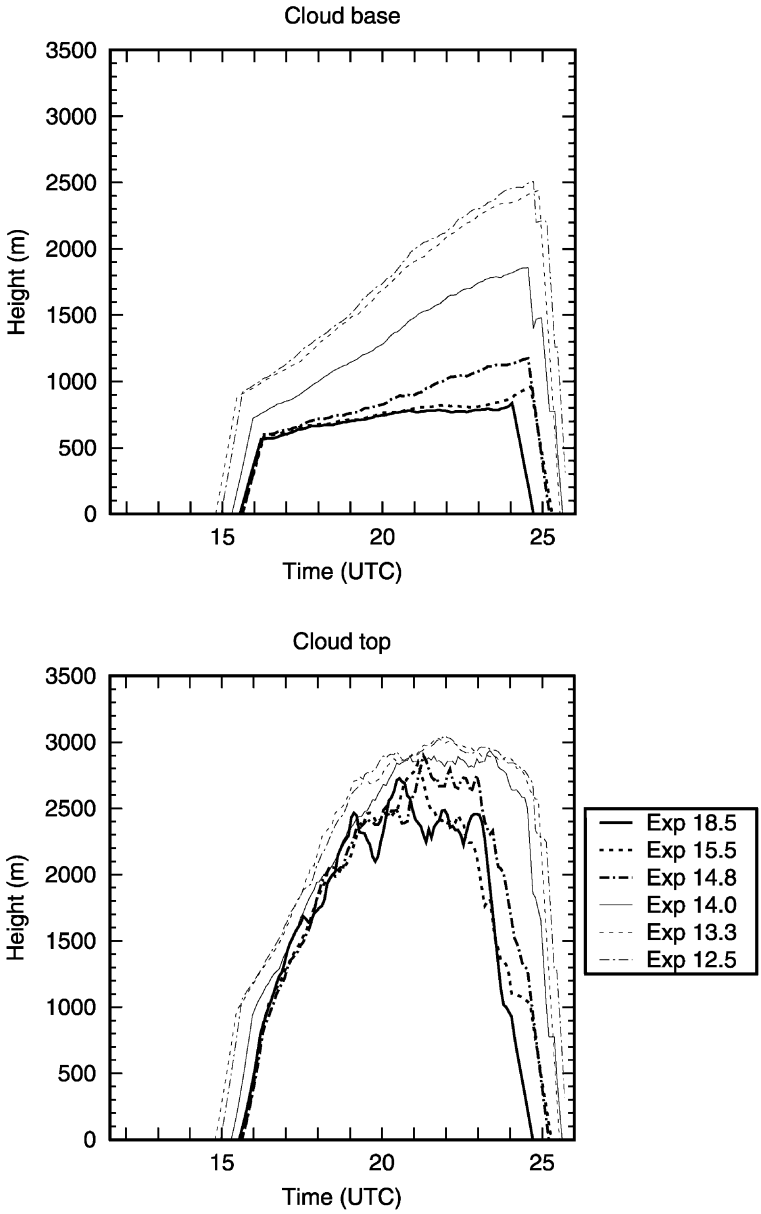

Fig. 5. Time evolution of minimum cloud base and maximum cloud top.

m difference between the onset of convection and the decay. Exp 14.8, which had surface fluxes most closely resembling observations, exhibits a 550 m change in cloud base, in good agreement with the observations as measured by the ceilometer and the

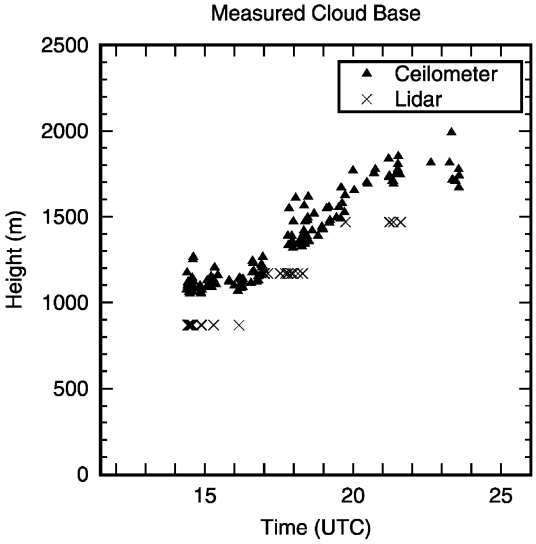

Fig. 6. Time evolution of measured cloud base at the ARM site using the Belfort ceilometer and micro-pulse lidar.

lidar. The actual values of cloud base are, however, lower in Exp 14.8 than in the observations. By definition, model cloud base is taken to be the lowest level where a non-zero value of cloud water exists, which is likely to be significantly lower than the instrument-measured values of cloud base. The changes in cloud base between the various experiments are a direct consequence of the surface heat flux partitioning, and therefore of the initial soil moisture content. As these fluxes transition from latent heat dominated to sensible heat dominated, the subcloud layer becomes increasingly warmer and drier, resulting in higher values of the lifting condensation level, and hence higher cloud bases.

The high sensitivity of cloud base height to initial soil moisture that was observed in this work could have a much broader impact. For example, Schär et al. (1999) studied

Table 3
Differences in cloud base height between the end and the beginning of cumulus convection for the sensitivity experiments and the measured cloud base values

Experiment	Cloud base height difference (m)
Exp 12.5	1500
Exp 13.3	1400
Exp 14.0	1100
Exp 14.8	550
Exp 15.5	350
Exp 18.5	250
Ceilometer	600
Lidar	600

the soil-precipitation feedback using month-long regional climate model simulations. They assessed the sensitivity of summertime European precipitation with respect to soil moisture using three different initial water contents: a reference field derived from ECMWF analysis, a dry experiment for which the soil water content was halved, and a wet experiment where it was doubled. The sensitivity in the precipitation field between the experiments was found to be in large part related to differences in the structure of the mean boundary layer between the dry and the wet experiments, with the dry experiments producing deep and dry boundary layers and the wet experiments shallow and moist layers. Nair et al. (submitted for publication) performed a numerical study of land use impact on the Costa Rican tropical cloud forest. They found that the effect of deforestation was to enhance surface sensible heat fluxes, leading to higher cloud base heights and thinner clouds. Data collected from various cloud forests around the world show that cloud droplet collection from orographic clouds by trees could represent a large fraction of the total precipitation. They postulated that the higher cloud base height over deforested areas might negatively impact the dry season water input. Our work complements these studies by indicating that small variations in soil moisture content can cause large variations in cloud base height, suggesting the importance of accurate soil moisture initialization in numerical simulations.

Domain-averaged vertical profiles for the two extreme simulations (Exp 18.5 and 12.5) as well as an intermediate case (Exp. 14.0) are shown in Fig. 7, between 2000 and 2100 UTC. Profiles of the potential temperature and total water mixing ratio show the impact of the surface fluxes on the subcloud layer. The dry simulation, Exp 12.5, has a subcloud layer that is nearly 5 K warmer and 5 g/kg drier than Exp 18.5. Exp 14.0 and the rest of the experiments (not shown) fall in between these two extreme cases. Also shown in Fig. 7 are the profiles of cloud fraction and cloud water. Despite very pronounced differences in cloud base, it is remarkable to note that the maximum values of cloud fraction and cloud water mixing ratio do not change dramatically among the three simulations.

To further assess the effect of soil moisture on the cloud morphology, we look at the maximum cloud fraction and liquid water path (LWP). Table 4 shows the maximum cloud fraction and LWP averaged between 1800 and 2100 UTC, corresponding to the peak in convective activity. The maximum cloud fraction always occurs near the cloud base. Values range between 11.0% for Exp 18.5 and 12.5% for Exp 14.0, representing a rather small variation. Furthermore, there is no systematic trend between cloud fraction and soil moisture. A trend is, however, noticeable for the LWP. The two driest experiments have LWP values of the order of 15 g/m^2, increasing to 24 g/m^2 for the simulation with highest soil moisture. To assess whether this change in LWP is a reflection of change in cloud water mixing ratio or merely a change in overall cloud depth, Table 4 also shows the average cloud depth during the 3-h period and the normalized LWP computed by taking the ratio of LWP and cloud depth. The values of the normalized LWP all fall within a relatively small range between 0.0140 and 0.0159 g/m^3, indicating that the increase in LWP with soil moisture is mostly a reflection of increased cloud depth.

Values of convective available potential energy (CAPE) computed using reversible adiabats are also shown in Table 4. The mean soundings for the dry simulations (Exp 12.5

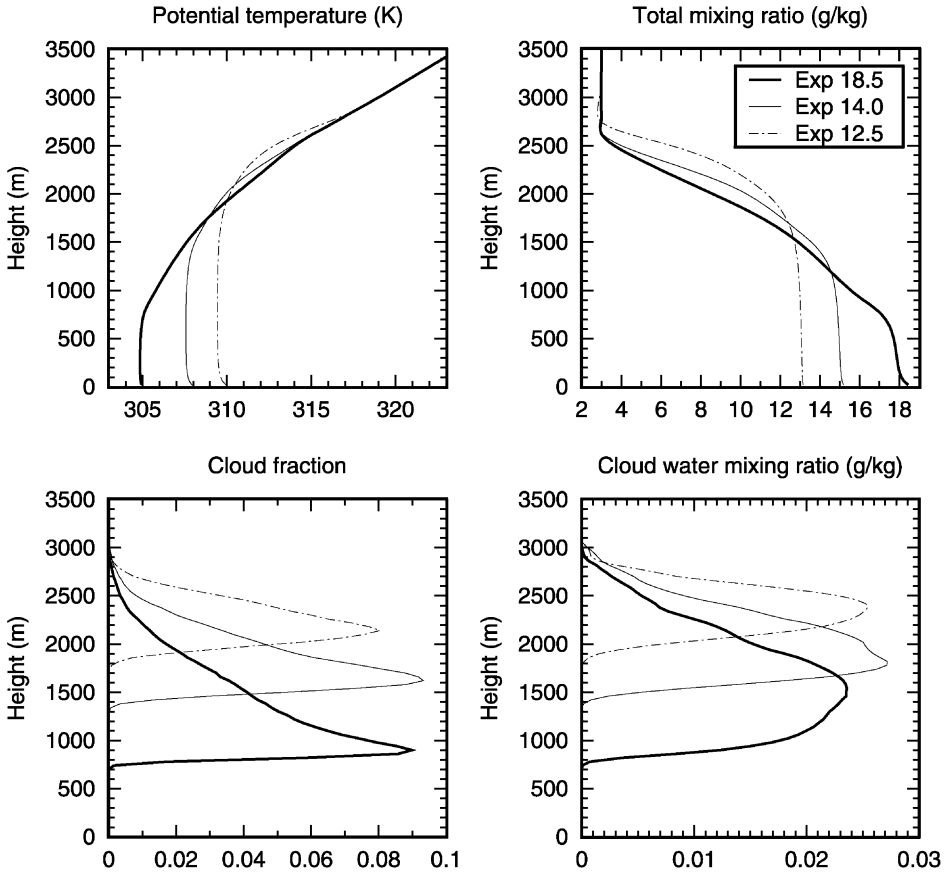

Fig. 7. Domain-averaged profiles of potential temperature, total water mixing ratio, cloud fraction and cloud water mixing ratio between 2000 and 2100 UTC for Exp. 18.5, 14.0, and 12.5.

and 13.3) have virtually no CAPE. This indicates that following the classification of Stull (1988), the clouds in these experiments would be classified as forced clouds. The moist experiments (Exp 14.8, 15.5, 18.5) have positive, albeit small values of CAPE. They might therefore be categorized as active clouds. The differences in CAPE are largely a consequence of very different subcloud layer equivalent potential temperature (θ_e) values (Table 4). The difference in low-level θ_e is an indirect consequence of the different EF between the experiments. Given a fixed amount of energy supplied to a volume of air, the change in θ_e is essentially independent of the partitioning between latent and sensible heat fluxes (Ashby, 2001). The change in low-level θ_e between the experiments is related to the growth rate of the subcloud layer, which is controlled by the amount of sensible heat flux. For large EF values, the boundary layer remains relatively shallow and the available energy is concentrated into a thin layer creating a larger increase in θ_e compared to dry conditions with low EF (Betts and Ball, 1995; Schär et al., 1999).

Table 4
Average values of maximum cloud fraction, LWP, cloud depth, cloud depth normalized LWP, CAPE, and low-level θ_e between 1800 and 2100 UTC

Experiment	Maximum cloud fraction (%)	LWP (g/m^2)	Cloud depth (m)	Normalized LWP (g/m^3)	CAPE (J/kg)	Low-level θ_e (K)
Exp 12.5	11.9	14.89	1010	0.0147	<1	343.7
Exp 13.3	11.3	15.01	1070	0.0140	<1	344.1
Exp 14.0	12.5	19.70	1240	0.0159	10.7	346.2
Exp 14.8	12.1	21.95	1480	0.0148	44.8	348.8
Exp 15.5	11.7	24.09	1595	0.0151	58.1	349.5
Exp 18.5	11.0	24.37	1580	0.0154	59.5	349.6

Finally, it is interesting to focus on the dynamics of the boundary layer and how it varies between experiments. For simplicity, we limit ourselves first to the two extreme cases: Exp 12.5 and 18.5. We use the maximum vertical velocity and average turbulence kinetic energy (TKE) to compare these experiments. Fig. 8 shows the maximum vertical velocity in the subcloud and cloud layers. Exp 18.5 exhibits large variations in maximum vertical velocity with values as high as 14 m/s in the cloud layer. The drier experiment has much smaller values of in-cloud w with maximum values around 8 m/s. The situation is reversed in the subcloud layer, where the maximum w values are observed in the driest experiment. It should not come as a surprise that the driest experiment produces a more active subcloud layer as higher sensible heat flux favors stronger thermals. Companion plots for the average TKE are shown in Fig. 9. As stated previously, the drier simulation, Exp 12.5, produces a much more vigorous subcloud layer with TKE values up to 3 m^2/s^2

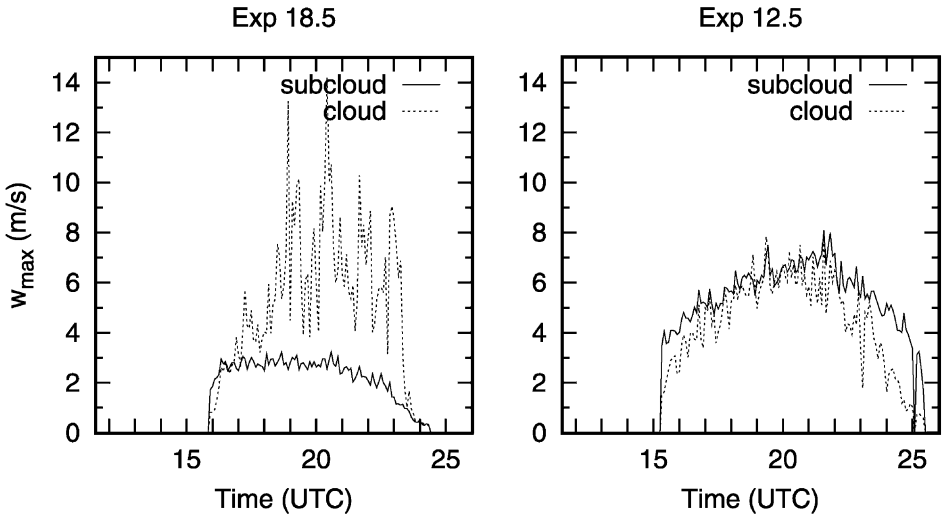

Fig. 8. Time evolution of domain maximum vertical velocity for the subcloud and cloud layers in Exp 18.5 and 12.5.

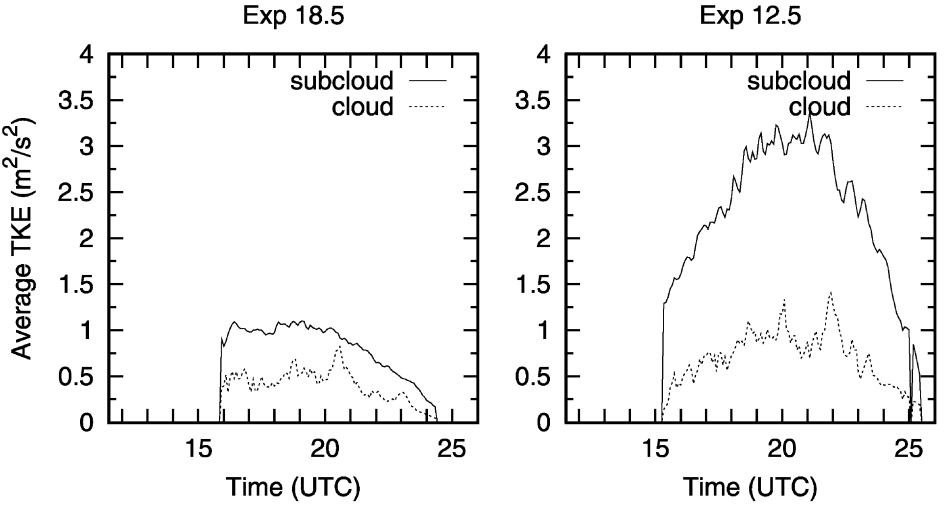

Fig. 9. Same as Fig. 8 but for average TKE.

compared to 1 m^2/s^2 for the moist simulation. However, the dry simulation also has higher average TKE values in the cloud layer as compared to Exp 18.5, and this despite the fact that the extreme values of w were much larger in Exp 18.5.

Further evidence of difference in boundary layer dynamics can be seen by looking at domain-averaged values of vertical velocity variance ($\overline{w'^2}$) and skewness for all sensitivity experiments. Fig. 10 shows $\overline{w'^2}$ averaged between 1800 and 2100 UTC. It is evident from

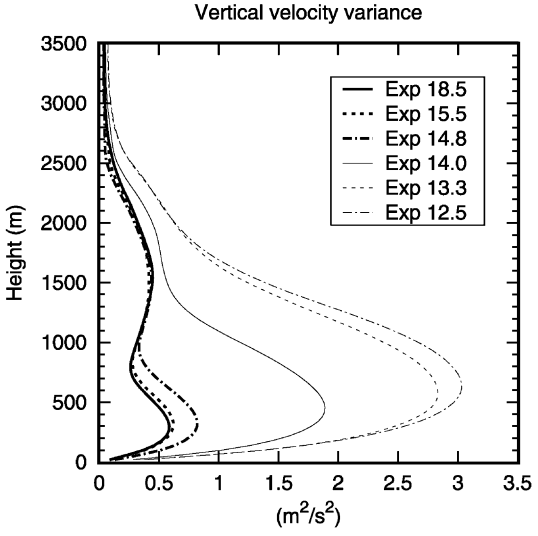

Fig. 10. Average vertical velocity variance for all experiments between 1800 and 2100 UTC.

this figure that the dry soil simulations, which produce much larger values of sensible heat fluxes, lead to a boundary layer with much stronger turbulence throughout the entire vertical domain. Differences are more pronounced in the subcloud layer. The vertical velocity skewness over the same time period is shown in Fig. 11. Particularly remarkable is the very large skewness value of 1.7 in the cloud layer for Exp 18.5. Exp 15.5 also exhibits a relatively large skewness value in the cloud layer, but smaller than Exp 18.5. These large skewness values indicate that the updrafts in these two simulations tend to be narrower and stronger than in the other experiments. Comparisons between vertical velocity variance and skewness confirm the findings from Figs. 8 and 9: drier simulations produce large values of sensible heat flux which in turn produce more vigorous boundary layers as measured by TKE and $\overline{w'^2}$. Experiments with higher soil moisture lead to latent heat dominated surface fluxes and less turbulence, but significantly larger extremes in cloud values of w as seen by the maximum w values and the large skewness.

It is interesting to contrast our findings with the sensitivity experiments of LLY1996 dealing with stratocumulus boundary layers. Compared to our simulations of cumulus clouds over land that were almost exclusively driven by surface fluxes, simulations of stratocumulus clouds are also very sensitive to cloud top long wave radiative cooling and cloud top entrainment instability. This makes a direct comparison between the results of LLY1996 and this work not possible, but some key findings can nevertheless be contrasted. LLY1996 found that surface sensible heat flux was much more efficient at generating buoyancy-driven turbulence. Simulations with relative high sensible heat input exhibited much larger values of vertical velocity variance in the subcloud layer than those with higher relative latent heat flux. This is very similar to what was found in this study (Fig. 10). They also observed that as the importance of surface latent heat flux increased, cloud fraction profiles exhibited a lower tail indicating a lower lifting

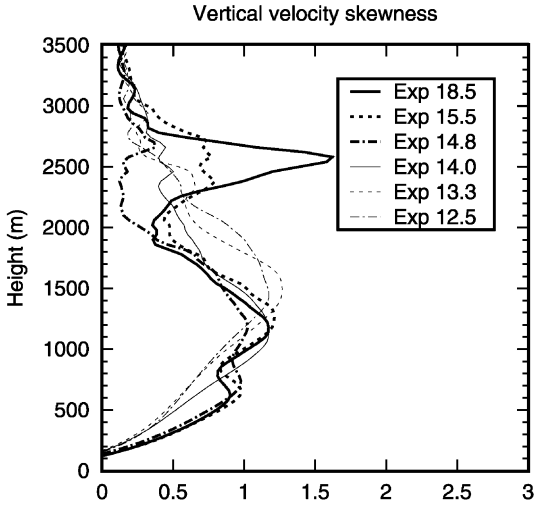

Fig. 11. Same as Fig. 10 but for vertical velocity skewness.

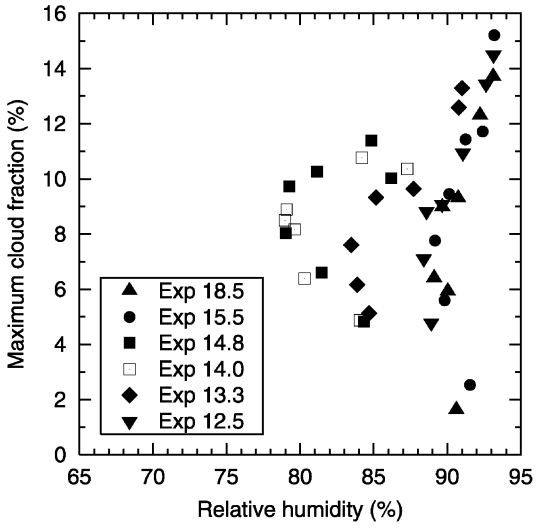

Fig. 12. Maximum cloud fraction as a function of relative humidity for hourly averages between 1700 and 2300 UTC for all simulations.

condensation level for the updrafts than for the cloud top radiatively generated downdrafts. The updrafts also tended to be fewer and stronger than those driven by surface sensible heat flux, similar to our moist simulations which had larger vertical velocity skewness values (Fig. 11).

LLY1996 observed fairly large differences in maximum cloud fraction between their various experiments, with values ranging from 41% to 95%. Even for simulations that differed only by their surface fluxes, significant variations in maximum cloud fraction existed. They furthermore found that a "nearly usable correlation" existed between the maximum cloud fraction and the relative humidity at the same level. This is in sharp contrast to this work where no systematic variation in maximum cloud fraction was observed among the various sensitivity experiments, despite large variations in surface heat fluxes. Our work indicates no useful correlation between cloud fraction and relative humidity. Fig. 12 shows the relationship between maximum cloud fraction and relative humidity at the same level for hourly averages between 1700 and 2300 UTC. Even though most of the highest cloud fraction values occur when the relative humidity is above 90%, no systematic trend is apparent. This is in sharp contrast with the findings of LLY1996 and could be of significant importance for cloud fraction parameterization schemes that use grid box average relative humidity as a predictor for cloud fraction.

5. Conclusion

A series of LES of non-precipitating cumulus clouds developing on top of a previously clear convective boundary layer were performed. These experiments were based on the 6th

GCSS boundary layer cloud working group intercomparison workshop case. The case was an idealization of observations made at the SGP ARM site on 21 June 1997. The various experiments differed by their initial soil moisture content ranging from 42% to 62% relative wetness. It was found that for the drier simulations, the surface fluxes were dominated by the sensible heat, whereas for the moister experiments, the latent heat flux dominated. The transition from sensible dominated to latent heat dominated fluxes was abrupt and occurred over a very narrow soil moisture range around 47% relative wetness. This abrupt transition was a result of the non-linearity of the vegetation stomatal conductance response function in LEAF-2 to the soil water potential.

The effect of this change in surface heat fluxes partitioning on the cloud field was mixed. Cloud base was significantly higher in the drier simulations leading to much shallower clouds as changes in cloud top were small. Soundings in the dry experiments had almost no CAPE, indicating that the clouds were essentially forced by the strong surface heating. The moister experiments had positive CAPE, leading to more convectively active clouds. Despite this large difference in forcing, maximum cloud fraction was essentially unchanged throughout all simulations with a value around 12% during midday. LWP increased as experiments became moister, but this increase in LWP appeared to be mostly related to an increase in overall cloud depth. Maximum cloud fraction was found to be uncorrelated with mean relative humidity, in contrast with the findings of LLY1996. This could have an important implication for cloud fraction parameterizations that use relative humidity as a predictor for cloud fraction. The dynamics of the cloudy boundary layer was very different between simulations with dominant sensible heat flux and those with dominant latent heat flux. Larger values of sensible heat flux led to more turbulent boundary layers, both in the subcloud and cloud layers. Latent heat flux dominated experiments exhibited much narrower and stronger updrafts in the cloud layer despite smaller average turbulence kinetic energy.

Acknowledgements

This work was supported by the National Science Foundation under grant ATM-9904128 and the National Oceanic and Atmospheric Administration under contract NA67RJ0152 AMEND 22. The US Department of Energy as part of the Atmospheric Radiation Measurement Program is acknowledged for providing access to its data archive. We are grateful to Robert L. Walko for his help with the LEAF-2 code. We also thank two anonymous reviewers for their precious comments on the manuscript.

References

Ashby, C.J., 2001. Impact of soil moisture initialization on a simulated flash flood. MSc Thesis, Colorado State University, Dept. of Atmospheric Science paper no. 702, Fort Collins, CO, USA.

Avissar, R., Pielke, R.A., 1991. The impact of plant stomatal control on mesoscale atmospheric circulations. Agricultural and Forest Meteorology 54, 353–372.

Avissar, R., Schmidt, T., 1998. An evaluation of the scale at which ground–surface heat flux patchiness affects the convective boundary layer using large-eddy simulations. Journal of the Atmospheric Sciences 55, 2666–2689.

Avissar, R., Eloranta, E.W., Gürer, K., Tripoli, G.J., 1998. An evaluation of the large-eddy simulation option of the Regional Atmospheric Modeling System in simulating a convective boundary layer: A FIFE case study. Journal of the Atmospheric Sciences 55, 1109–1130.

Betts, A.K., Ball, J.H., 1995. The FIFE surface diurnal cycle climate. Journal of Geophysical Research 100, 25679–25693.

Brown, A.R., 1999. The sensitivity of large-eddy simulations of shallow cumulus convection to resolution and subgrid model. Quarterly Journal of the Royal Meteorological Society 125, 469–482.

Chen, F., Avissar, R., 1994. Impact of land–surface moisture variability on local shallow convective cumulus and precipitation in large-scale models. Journal of Applied Meteorology 33, 1382–1401.

Cotton, W.R., Pielke Sr., R.A., Walko, R.L., Liston, G.E., Tremback, C.J., Jiang, H., McAnelly, R.L., Harrington, J.Y., Nicholls, M.E., 2001. RAMS 2001: Current status and future directions. Meteorology and Atmospheric Physics, submitted for publication.

Cuijpers, J.W.M., Duynkerke, P.G., 1993. Large eddy simulation of trade wind cumulus clouds. Journal of the Atmospheric Sciences 50, 3894–3908.

Cuijpers, J.W.M., Duynkerke, P.G., Nieuwstadt, F.T.M., 1996. Analyses of variance and flux budgets in cumulus-topped boundary layers. Atmospheric Research 40, 307–337.

Deardorff, J.W., 1972. Numerical investigation of neutral and unstable planetary boundary layers. Journal of the Atmospheric Sciences 29, 91–115.

Deardorff, J.W., 1974. Three-dimensional numerical study of turbulence in an entraining mixed layer. Boundary-Layer Meteorology 7, 199–226.

Deardorff, J.W., 1980. Stratocumulus-capped mixed layers derived from a three-dimensional model. Boundary-Layer Meteorology 18, 495–527.

Harrington, J.Y., 1997. The effects of radiative and microphysical processes on simulated warm and transition arctic stratus. PhD Dissertation, Colorado State University, Dept. of Atmospheric Science paper no. 637, Fort Collins, CO, USA.

Lee, T.J., 1992. The impact of vegetation on the atmospheric boundary layer and convective storms. PhD Dissertation, Colorado State University, Dept. of Atmospheric Science Paper No. 509, Fort Collins, CO, USA.

Lewellen, D.C., Lewellen, W.S., Yoh, S., 1996. Influence of Bowen ratio on boundary-layer cloud structure. Journal of the Atmospheric Sciences 53, 175–187.

Mason, P.J., 1994. Large-eddy simulation: a critical review of the technique. Quarterly Journal of the Royal Meteorological Society 120, 1–26.

Moeng, C.-H., 1984. A large-eddy simulation model for the study of planetary boundary-layer turbulence. Journal of the Atmospheric Sciences 41, 2052–2062.

Moeng, C.-H., Wyngaard, J.C., 1984. Statistics of conservative scalars in the convective boundary layer. Journal of the Atmospheric Sciences 41, 3161–3169.

Moeng, C.-H., Wyngaard, J.C., 1988. Spectral analysis of large-eddy simulations of the convective boundary layer. Journal of the Atmospheric Sciences 45, 3573–3587.

Moeng, C.-H., Cotton, W.R., Bretherton, C., Chlond, A., Khairoutdinov, M., Krueger, S., Lewellen, W.S., MacVean, M.K., Pasquier, J.R.M., Rand, H.A., Siebesma, A.P., Stevens, B., Sykes, R.I., 1996. Simulation of a stratocumulus-topped planetary boundary layer: Intercomparison among different numerical codes. Bulletin of the American Meteorological Society 77, 261–278.

Nair, U.S., Lawton, R.O., Welch, R.M., Pielke Sr., R.A., 2001. Impact of land use on Costa Rican tropical montane cloud forests: 1. Sensitivity of cumulus cloud field characteristics to lowland deforestation. Journal of Geophysical Research, submitted for publication.

Pielke Sr., R.A., 2001. Influence of the spatial distribution of vegetation and soils on the prediction of cumulus convective rainfall. Reviews of Geophysics 39, 151–177.

Pielke, R.A., Cotton, W.R., Walko, R.L., Tremback, C.J., Lyons, W.A., Grasso, L.D., Nicholls, M.E., Moran, M.D., Wesley, D.A., Lee, T.J., Copeland, J.H., 1992. A comprehensive meteorological modeling system RAMS. Meteorology and Atmospheric Physics 49, 69–91.

Schär, C., Lüthi, D., Beyrle, U., Heise, E., 1999. The soil-precipitation feedback: A process study with a regional climate model. Journal of Climate 12, 722–741.

Schmidt, H., Schumann, U., 1989. Coherent structure of the convective boundary layer derived from large-eddy simulations. Journal of Fluid Mechanics 200, 511–562.

Stull, R.B., 1988. An Introduction to Boundary Layer Meteorology. Kluwer Academic Publishers, Dordrecht, The Netherlands, 666 pp.

Walko, R.L., Cotton, W.R., Meyers, M.P., Harrington, J.Y., 1995. New RAMS cloud microphysics parameterization: Part I. The single-moment scheme. Atmospheric Research 38, 29–62.

Walko, R.L., Band, L.E., Baron, J., Kittel, T.G.F., Lammers, R., Lee, T.J., Ojima, D., Pielke Sr., R.A., Taylor, C., Tague, C., Tremback, C.J., Vidale, P.L., 2000. Coupled atmosphere–biophysics–hydrology models for environment modeling. Journal of Applied Meteorology 39, 931–944.